Remote Sensing of Environment 183 (2016) 226–238

Contents lists available at ScienceDirect

Remote Sensing of Environment

journal homepage: www.elsevier.com/locate/rse

Quantifying the influences of spectral resolution on uncertainty in leaf trait estimates through a Bayesian approach to RTM inversion

Alexey N. Shiklomanov [a,*], Michael C. Dietze [a], Toni Viskari [b,c], Philip A. Townsend [d], Shawn P. Serbin [b,c]

[a] Department of Earth & Environment, Boston University, Boston, MA, USA
[b] Environmental & Climate Sciences Department, Brookhaven National Laboratory, Upton, NY, USA
[c] Sustainability Studies, Stony Brook University, Stony Brook, NY, USA
[d] Department of Forest and Wildlife Ecology, University of Wisconsin-Madison, Madison, WI, USA

ARTICLE INFO

Article history:
Received 4 October 2015
Received in revised form 18 May 2016
Accepted 28 May 2016
Available online xxxx

Keywords:
Leaf optical properties
PROSPECT
Radiative transfer modeling
Hyperspectral data
Bayesian statistics
Spectral inversion

ABSTRACT

The remote monitoring of plant canopies is critically needed for understanding of terrestrial ecosystem mechanics and biodiversity as well as capturing the short- to long-term responses of vegetation to disturbance and climate change. A variety of orbital, sub-orbital, and field instruments have been used to retrieve optical spectral signals and to study different vegetation properties such as plant biochemistry, nutrient cycling, physiology, water status, and stress. Radiative transfer models (RTMs) provide a mechanistic link between vegetation properties and observed spectral features, and RTM spectral inversion is a useful framework for estimating these properties from spectral data. However, existing approaches to RTM spectral inversion are typically limited by the inability to characterize uncertainty in parameter estimates. Here, we introduce a Bayesian algorithm for the spectral inversion of the PROSPECT 5 leaf RTM that is distinct from past approaches in two important ways: First, the algorithm only uses reflectance and does not require transmittance observations, which have been plagued by a variety of measurement and equipment challenges. Second, the output is not a point estimate for each parameter but rather the joint probability distribution that includes estimates of parameter uncertainties and covariance structure. We validated our inversion approach using a database of leaf spectra together with measurements of equivalent water thickness (EWT) and leaf dry mass per unit area (LMA). The parameters estimated by our inversion were able to accurately reproduce the observed reflectance ($RMSE_{VIS} = 0.0063$, $RMSE_{NIR\text{-}SWIR} = 0.0098$) and transmittance ($RMSE_{VIS} = 0.0404$, $RMSE_{NIR\text{-}SWIR} = 0.0551$) for both broadleaved and conifer species. Inversion estimates of EWT and LMA for broadleaved species agreed well with direct measurements ($CV_{EWT} = 18.8\%$, $CV_{LMA} = 24.5\%$), while estimates for conifer species were less accurate ($CV_{EWT} = 53.2\%$, $CV_{LMA} = 63.3\%$). To examine the influence of spectral resolution on parameter uncertainty, we simulated leaf reflectance as observed by ten common remote sensing platforms with varying spectral configurations and performed a Bayesian inversion on the resulting spectra. We found that full-range hyperspectral platforms were able to retrieve all parameters accurately and precisely, while the parameter estimates of multispectral platforms were much less precise and prone to bias at high and low values. We also observed that variations in the width and location of spectral bands influenced the shape of the covariance structure of parameter estimates. Our Bayesian spectral inversion provides a powerful and versatile framework for future RTM development and single- and multi-instrumental remote sensing of vegetation.

1. Introduction

The terrestrial biosphere is fundamentally dependent on the interactions between plants and solar radiation through photosynthesis. Consequently, we can learn a lot about the structure and functioning of ecosystems by studying these interactions in detail, and over the last several decades our capability do so has expanded dramatically. Specifically, global scale remote sensing observations from satellites such as Landsat, MODIS, and AVHRR have been used to map and monitor vegetation productivity, distribution, and abundance at high temporal frequency (Loveland et al., 2000; Friedl et al., 2002; Hansen, Stehman, & Potapov, 2010; Houborg, Fisher, & Skidmore, 2015). At the landscape scale, satellite and sub-orbital (airborne) platforms with high spatial (e.g. WorldView, <1 m) and/or spectral (e.g. AVIRIS Classic, 10 nm) resolution sensors have been able to quantify the spatial distribution of canopy structure, nutrient status, and species composition (Asner, Martin, Anderson, & Knapp, 2015; Banskota et al., 2015; Singh, Serbin, McNeil, Kingdon, & Townsend, 2015). In addition, field spectrometers with the highest available spectral resolution have provided a fast and

* Corresponding author.
E-mail address: ashiklom@bu.edu (A.N. Shiklomanov).

http://dx.doi.org/10.1016/j.rse.2016.05.023
0034-4257/

relatively simple method for characterizing and monitoring leaf physiology, biochemistry, and morphology (Serbin, Dillaway, Kruger, & Townsend, 2012; Couture, Serbin, & Townsend, 2013; Sullivan et al., 2013; Serbin, Singh, McNeil, Kingdon, & Townsend, 2014; Zhao et al., 2014).

An important caveat of using spectral information to study vegetation is that the optical properties being measured are often not of primary interest. Rather, we are interested in physiologically or ecologically meaningful variables such as total biomass, photosynthetic efficiency, species composition, biomass, or biochemistry that drive observed spectral signatures of vegetation (Curran, 1989) and which can be inferred from the optical properties. This connection is usually made empirically, either by simple regression with spectral vegetation indices (SVIs) (Fassnacht, Stenzel, & Gitelson, 2015; Haboudane, Miller, Tremblay, Zarco-Tejada, & Dextraze, 2002; Huete et al., 2002) or through more advanced statistical methods such as partial least squares regression (PLSR) (Couture et al., 2013; Serbin et al., 2012, 2014; Singh et al., 2015) and wavelet transforms (Banskota, Wynne, Serbin, Kayastha, & Townsend, 2013; Blackburn & Ferwerda, 2008; Cheng, Rivard, Sánchez-Azofeifa, Feng, & Calvo-Polanco, 2010). However, these approaches can have important limitations depending on the application. First, the empirical nature of these methods can result in sensor, site, and/or vegetation specific relationships, as evidenced by the substantial variability in coefficients and choice of wavelengths across studies (Croft, Chen, & Zhang, 2014; Huete et al., 2002; Knyazikhin et al., 1998; Leprieur, Verstraete, & Pinty, 1994; Liu, Pattey, & Jégo, 2012; Myneni et al., 2002; Wessels, van den Bergh, & Scholes, 2012). Second, empirical approaches are not a direct mechanistic relationship between spectra and plant properties and therefore do not provide the true connections between optical properties and variables of interest (Knyazikhin et al., 2013). As a result, extrapolating empirical approaches and relationships to larger regions or new locations can be challenging. Moreover, the indirect, derived data products that arise from such analyses may have a limited capacity to inform ecosystem models (Quaife et al., 2008), as they often introduce assumptions that conflict with the internal logic of the processes represented in these models.

In contrast, radiative transfer models (RTMs), which provide a more mechanistic link between plant traits and spectral signatures, can be a useful alternative to empirical approaches. A variety of standalone RTMs exist from the leaf (Dawson, Curran, & Plummer, 1998; Feret et al., 2008; Ganapol, Johnson, Hammer, Hlavka, & Peterson, 1998) to canopy scales (Jacquemoud et al., 2009; Kuusk, 2001; Verhoef, 1984; Wang & Li, 2013). In addition, RTMs are often an important component of dynamic vegetation models, where they are used to calculate surface energy balance and light availability for photosynthesis (Medvigy, Wofsy, Munger, Hollinger, & Moorcroft, 2009; Ni-Meister, Yang, & Kiang, 2010; Kobayashi et al., 2012). In this study, we focus on the leaf-level PROSPECT model (Jacquemoud & Baret, 1990), which has been extensively used in forward (simulation) mode to develop and test new remote sensing techniques (Croft et al., 2014; Féret et al., 2011; Hunt, Wang, Qu, & Hao, 2012; Le Maire, François, & Dufrêne, 2004; Zarco-Tejada et al., 2013) as well as to estimate leaf traits from spectral observations via inversion (Atzberger & Richter, 2012; Feret et al., 2008; Jacquemoud, Baret, Andrieu, Danson, & Jaggard, 1995; Jacquemoud et al., 2009; Li & Wang, 2013; Li & Wang, 2011; Zarco-Tejada et al., 2004). However, the commonly used approaches for RTM inversion—such as least-squares minimization and look-up tables—fail to directly quantify the uncertainties and account for the correlations among the resulting parameter estimates. The characterization of uncertainty is a fundamental requirement for drawing meaningful scientific conclusions from results and for assimilating results into statistical or mechanistic models (Cressie, Calder, Clark, Ver Hoef, & Wikle, 2009; Quaife et al., 2008).

Applying Bayesian statistics to RTM inversion activities provides a direct means to quantify the uncertainty and covariance of parameter estimates while combining multiple sources of information. The use of independent prior information has been a critical component of RTM inversion as a way to solve the otherwise underdetermined problem of estimating a large number of RTM parameters from a small number of observations (Combal et al., 2003; Lauvernet, Baret, Hascoët, Buis, & Le Dimet, 2008; Yao, Liu, Liu, & Li, 2008; Pinty et al., 2011; Zhang et al. 2012; Laurent, Schaepman, Verhoef, Weyermann, & Chávez, 2014; Mousivand, Menenti, Gorte, & Verhoef, 2015). While these studies either neglect parameter uncertainty or estimate it using computationally-efficient approximations (e.g. Gaussian posterior distributions), recent work has demonstrated the efficacy of fully-Bayesian Markov Chain Monte Carlo (MCMC) approaches for inversion of the PROSAIL canopy RTM using MODIS (and "MODIS-like") data (Zhang et al., 2005, 2006; Zhang et al., 2009, & 2011). However, to the authors' knowledge, such approaches have yet to be applied to hyperspectral data, neither at the canopy nor the leaf scales. A recent study by Lepine, Ollinger, Ouimette, and Martin (2016) further demonstrated that PLSR estimates of canopy nitrogen are less sensitive to spectral resolution than spatial resolution and sensor fidelity, but no comparable analyses has been attempted for other foliar constituents, nor, for that matter, using a physically-based RTM rather than an empirical regression. In this study, we examine the effects of measurement spectral characteristics on accuracy, uncertainty, and covariance of leaf traits estimated from spectral inversion of a leaf RTM. First, we demonstrate the applicability of a fully Bayesian approach to leaf RTM inversion and validate this approach using data from the NASA Forest Functional Types (FFT) database of field spectra (Serbin et al., 2014; Singh et al., 2015). Second, we simulate reflectance observations using the spectral response functions of ten common remote sensing platforms and test the accuracy and precision with which our inversion algorithm can retrieve parameters from these observations. Although such an experiment is highly idealized, it does provide insight on the absolute theoretical limits of RTM inversion by different remote sensing platforms and illustrates how subtle changes in spectral measurement characteristics can affect inversion results. More broadly, this work reiterates the power of a Bayesian framework for fully utilizing the vast archive of remote sensing and field spectral observations to enhance our understanding of ecosystem processes.

2. Methods

2.1. Inversion procedure

The PROSPECT 5 model simulates the full spectral reflectance and transmittance of a leaf over the 400–2500 nm range using five key parameters related to leaf structure and biochemistry (Feret et al., 2008). In the PROSPECT model, a leaf is treated as a set of N partially transparent flat plates, each with wavelength-dependent transmissivity k_λ. Transmissivity k_λ is based on the linear combination of empirically calibrated specific absorption spectra for total chlorophyll (a and b), total carotenoids, water, and dry matter (e.g. cellulose, lignin, protein) multiplied by their respective quantities (given by the parameter values: Cab, Car, Cw, Cm) (Table 1; Fig. S1). For further detail on the PROSPECT model, see Feret et al. (2008).

The objective of RTM spectral inversion is to estimate the physical RTM parameters from the observed spectral information. This is accomplished through a statistical inversion, wherein we seek the set of parameters that minimizes the residual error between PROSPECT-modeled and measured reflectance. Our approach to the inversion of PROSPECT is distinct from previous studies (Combal et al., 2003; Feret et al., 2008; Féret et al., 2011; Li & Wang, 2011, 2013) in two important ways. First, whereas many past studies use both reflectance and transmittance to estimate parameters, we use only reflectance. Reflectance is generally easier to measure than transmittance, which requires special instrumentation such as integrating spheres that often have inadequate designs and yield poor signal-to-noise ratios, especially in the

Table 1
Summary of PROSPECT 5 parameters. Ranges for Car, Cw, and Cm are based on the datasets used for their calibration (ANGERS for Cab and Car, LOPEX for Cw and Cm) as reported in Feret et al. (2008). The ranges for N and Cab are calculated from the LOPEX and ANGERS databases, respectively (available online at http://opticleaf.ipgp.fr or on request). Units for Cw and Cm are adjusted for readability (original units are g cm^{-2}).

Parameter	Description	Unit	Range
N	Structural parameter; effective number of mesophyll layers	Unitless	1.09 to 3.00
Cab	Total chlorophyll (*a* and *b*) density	μg cm^{-2}	0.78 to 106.72
Car	Total carotenoid density	μg cm^{-2}	0 to 25.3
Cw	Equivalent water thickness	g m^{-2}	43 to 439
Cm	Leaf dry matter content per unit area	g m^{-2}	17 to 152

longer wavelengths (i.e. >2 μm). As well, inversion on reflectance data alone allows transmittance measurements as optional data for independent validation. Second, unlike past leaf-level PROSPECT inversion studies that only provide point estimates of parameters, we performed our analysis within a Bayesian framework that provides the joint probability distribution of the PROSPECT 5 parameters, $\theta = \{N, Cab, Car, Cw, Cm\}$, and the residual standard deviation, σ, as the output. The general mathematical statement of this posterior distribution is given as follows:

$$P(\theta, \sigma | X) \propto P(X | \theta, \sigma)\, P(\theta)\, P(\sigma)$$
$$P(X | \theta, \sigma) \sim \text{Normal}(\text{PROSPECT5}(\theta) | X, \sigma),$$

where PROSPECT5(θ) is the modeled reflectance given θ, and X is a vector of observed reflectance values. The residual error is assumed to be normally distributed with a mean of 0 and standard deviation of σ.

We set the prior distribution for N to a lognormal distribution shifted to have a minimum of 1, and parameterized based on a review of literature using the PROSPECT model (Le Maire et al., 2004; Ferreira, Grondona, Rolim, & Shimabukuro, 2013; Croft et al., 2014) (Fig. S2). We assigned the remaining parameters log-normal priors based on summary statistics and histograms from the LOPEX, ANGERS, HAWAII, and CALMIT spectral databases as reported by Feret et al. (2008) (Fig. S2). The residual variance σ^2 was assigned an uninformative inverse gamma prior, which is conjugate with the normal distribution and therefore allows for computationally efficient Gibbs sampling.

We sampled the joint posterior distribution of the PROSPECT 5 parameters using the Metropolis-Hastings (MH) algorithm with adaptive block sampling (Haario, Saksman, & Tamminen, 2001). For this, we initialized each inversion using parameter values drawn at random from the prior distributions. For each inversion, we ran the algorithm five times (i.e. five independent chains) for 100,000 iterations each. At each iteration, the algorithm proposes a parameter vector, calculates the vector's likelihood based on the observations and the prior, and accepts or rejects the vector based on this likelihood. The proposal step performs a random draw from a multivariate normal distribution centered on the last accepted parameter vector. The covariance matrix for the multivariate normal proposal distribution was re-computed every 100 iterations as follows: (1) the univariate standard deviation of each parameter and the Pearson product-moment correlation matrix were computed; (2) the standard deviation vector was multiplied by the ratio of the acceptance rate in the last 100 samples to the target acceptance rate (set to 0.234, as per Haario et al., 2001); (3) the resulting standard deviation vector was converted to a diagonal matrix and multiplied to both sides of the correlation matrix to give a re-scaled covariance matrix. For each inversion, we determined MCMC convergence based on a value of the Gelman-Rubin multivariate potential scale reduction factor of less than 1.1 (Gelman & Rubin, 1992, as implemented in the R *coda* package v.0.18–1 by Plummer et al., 2016). For runs that did not converge, we repeated this process with a 20% smaller target acceptance rate for the adaptation step, which increases the size of the sampling space for each chain and therefore reduces the likelihood of getting trapped in local minima. Across the >10,000 inversions performed in this study, only five failed to converge (after five inversion attempts)—all for simulated CHRIS-Proba spectra (see Section 2.3)—and we excluded these data points from our analysis. We visually examined a random subset of the resulting trace plots and autocorrelograms and determined that a common burn-in period of 80,000 samples and a thinning interval of 20 was sufficient for an accurate and representative sample of the joint posterior distribution. After applying the burn-in and thinning filter, we calculated the mean, standard deviation, and 95% confidence intervals of the sampled parameter values (Fig. S3).

With chains running in parallel, the inversion of one leaf spectrum with our specifications takes approximately 4 min (on one Intel® Xeon™ X5570 CPU @ 2.93GHz), and running the entire set of over 10,000 inversions required for this paper took several days (running up to 16 inversions simultaneously on a high performance computing cluster). That being said, we anticipate that recoding of the algorithm from R to a compiled language will dramatically increase (>50×) the computational efficiency of our approach.

The inversion algorithm described above is available as an open-source, publicly-available R (R Development Core Team, 2008) package housed within the PEcAn ecoinformatics toolbox (github.com/pecanproject/pecan/tree/master/modules/rtm) (Dietze, Lebauer, & Kooper, 2013; LeBauer, Wang, Richter, Davidson, & Dietze, 2013). This package allows users to simulate spectra using the PROSPECT family of radiative transfer models and apply our inversion algorithm to their own models and data. For more information, refer to the package vignette on the PEcAn tutorials page (pecanproject.github.io/tutorials.html).

2.2. Validation

2.2.1. Data

We tested the ability of our inversion to accurately estimate leaf traits using data collected as part of the NASA Forest Functional Types (FFT) campaign (Deel et al., 2012; Serbin et al., 2014; Singh et al., 2015). This dataset consists of leaves collected from various positions within the canopy for 52 species from 13 sites across the Northeast and Midwest USA. An Analytical Spectral Devices (ASD) FieldSpec 3 Full Range (350 to 2500 nm) spectroradiometer was used together with a leaf clip and internal calibrated light source to measure reflectance on the adaxial surface of 1348 unique leaves. For a subset of 765 of these leaves, the same instrument was used with an ASD integrating sphere setup to measure transmittance through the leaf adaxial surface. Our database included both broadleaf and conifer species. For conifer measurements, we constructed edge-to-edge mats of needles larger than the spot size of the light source (Serbin, 2012; Singh et al., 2015). As detailed in Serbin (2012), we found minimal changes in reflectance/transmittance measurement up to a threshold of differing gaps between needles. These observations are henceforth referred to as "FFT measured reflectance and transmittance," respectively. In addition to spectral measurements, laboratory measurements of leaf dry mass per unit area (LMA) and equivalent water thickness (EWT) were available for 950 leaves. For further information on the sampling methodology, see Serbin et al. (2014).

During exploratory analysis, we observed that inversion results by leaf habit displayed some distinct differences and conifer species were consistently less accurate than results for broadleaved species, reflecting ecological differences in leaf structure that are not well represented by the PROSPECT model. Therefore, to better contextualize our results, we performed both validation steps for the entire data set and

separately for broadleaved and conifer species. However, even within the conifer functional type, we found certain species and foliar morphologies showed much larger errors than others. These differences could be ecological in nature or an artifact related to the challenges of measuring full-range reflectance and transmittance of different types of conifer needles. To investigate whether these errors aligned with established ecological classifications, we grouped species based on their approximate succession ("early", "mid", or "late"), following the general classification scheme of Dietze and Moorcroft (2011), except that we grouped the "Northern" and "Southern Pine" functional types as "early conifer." Classification based on succession is useful for this study because it is indicative of plant shade tolerance (Dietze & Moorcroft, 2011), which is closely linked to leaf structure and biochemistry (Poorter, Niinemets, Poorter, Wright, & Villar, 2009).

We applied our inversion algorithm individually to each of the FFT measured reflectance spectra ($n = 1348$), resulting in an estimate of the joint probability distribution of the PROSPECT 5 parameters for each leaf. We then generated a dataset of synthetic reflectance spectra ("FFT simulated reflectance") by using the middle 90% of these parameter estimates ($n = 1040$) as inputs to the PROSPECT 5 model. These synthetic reflectance spectra were used as data in the sensor simulation experiment (Section 2.3). We used real parameter estimates rather than random draws from a distribution to preserve their ecological ranges and covariances resulting from within- and between-species tradeoffs in traits such as those described for the leaf economics spectrum (Wright et al., 2004).

We then performed two different tests to evaluate the accuracy of these parameter estimates: (1) We compared the FFT simulated reflectance and transmittance to measured reflectance and transmittance, and (2) we directly compared the inversion estimates of PROSPECT 5 parameters Cw and Cm to measured values of EWT and LMA, respectively.

2.2.2. Reflectance and transmittance

A common way to validate model inversion is to run the model in forward mode using the estimated parameters as inputs and compare the output to the original data. For our study, we used the inversion estimates of the PROSPECT parameters as inputs to the PROSPECT model to predict reflectance and transmittance spectra, which we then compared to the observed reflectance and transmittance. Errors in spectral inversion can originate from multiple sources, including measurement error (both trait and spectra), failure of the PROSPECT model to fully capture leaf spectral features (i.e. model formulation error), and parameter identifiability issues in the inversion algorithm. To isolate algorithmic error, we first performed the validation on a set of synthetic reflectance and transmittance spectra ($n = 1348$). To investigate the remaining sources of error, we performed the same validation on FFT measured reflectance ($n = 1348$) and transmittance ($n = 765$) spectra. For both reflectance and transmittance, we calculated the mean and 90% and 95% confidence intervals on the absolute error (simulated - measured) at each wavelength. The overlap of the 95% confidence interval with 0 was used to judge statistical significance. To facilitate comparison with other RTM inversion studies (Feret et al., 2008; Di Vittorio, 2009a), we also computed the root mean square error (RMSE), bias (BIAS), and bias-corrected RMSE (SEPC) averaged across the visible (VIS, 400–800 nm) and near-infrared (NIR, 801–2500 nm) regions of the spectrum:

$$RMSE = \sqrt{\frac{\sum_i^n (x_i - x_o)^2}{n}}$$
$$BIAS = \frac{\sum_i^n (x_i - x_o)}{n}$$
$$SEPC = \sqrt{\frac{\sum_i^n (x_i - x_o - BIAS)^2}{n}},$$

where x_i is the simulated value (reflectance or transmittance), x_o is the observed value, and n is the number of spectra considered.

2.2.3. EWT and LMA

For leaves that had paired measurements of reflectance and EWT and LMA ($n = 950$), we compared the mean inversion estimates for PROSPECT parameters Cw and Cm to measured values of EWT and LMA, respectively. For each, we compared the mean inversion estimate to the measured value via the RMSE, BIAS, and SEPC as above (with inversion estimate x and measurement x_o) as well as relative RMSE (RMS%E) and the relative bias-corrected RMSE (CV):

$$RMS\%E = \sqrt{\frac{\sum_i^n \left(\frac{x_i - x_o}{x_o}\right)^2}{n}} \times 100\%$$
$$CV = \frac{SEPC}{x_{obs}} \times 100\%$$

2.3. Sensor simulation experiment

Recent work has shown that PLSR estimates of foliar nitrogen content are less sensitive to spectral resolution than to other factors such as spatial resolution and sensor fidelity (Lepine et al., 2016). However, the PLSR approach implemented in that study was unable to quantify the uncertainty around the nitrogen estimates. We hypothesize that the spectral characteristics of most common remote sensing platforms are sufficient to accurately estimate the leaf biophysical parameters modeled by PROSPECT, but that the uncertainties in these parameters will increase with declining spectral resolution. To test this hypothesis, we transformed the FFT simulated reflectance spectra using the relative spectral response functions of 11 common remote sensing platforms (Table 2, Fig. S4), and used our Bayesian inversion of PROSPECT 5 to retrieve the starting parameters from the transformed spectra. For input parameters, we used the inversion results from measured spectra, thereby capturing a large range of ecologically realistic values and preserving inherent covariances between parameters. To account for observation error, we simulated Gaussian random noise (with mean 0 and standard deviation 2.5×10^{-4}) smoothed with a Gaussian filter (kernel width 11) to account for inherent autocorrelation in hyperspectral measurements (Fig. S5).

We then examined how two characteristics of the inversions varied between sensors: Relative bias (α) indicates how closely the mean parameter estimate (μ) matched the true value (p) and is a useful measure for describing the accuracy of the estimate's central tendency.

$$\alpha = \frac{\mu - p}{p}$$

Uncertainty (π) describes the width of the 95% confidence interval of the estimate (s) relative to the mean value, and is useful for ascertaining the precision with which the inversion is able to estimate a parameter.

$$\pi = \frac{s}{\mu}$$

We note that both statistics are normalized to facilitate inter-parameter comparison. Both metrics were computed for each parameter for each inversion and then averaged over all simulated spectra.

We recognize that this experiment does not fully capture all of the variability associated with inversion of real observations from these sensor systems given its failure to account for canopy structure,

Table 2
Spectral, spatial, and temporal characteristics of several important previous and current remote sensing platforms and instruments considered in the sensor simulation experiment.

Sensor	Number of Bands	Spectral range (nm)	Bandwidth (nm)	Spatial resolution (m)	Revisit time (days)
AVIRIS NG	416	380 to 2510	5	0.3 to 4.0[a]	On-demand
AVIRIS Classic	216	400 to 2500	10	<10 to 20[a]	On-demand
CHRIS-Proba	62	410 to 1050	1.5 to 12	36	7 to 8
Hyperion	225	350 to 2500	10	30	16
Landsat 5 (TM)	6	450 to 2350	60 to 270	30	16
Landsat 7 (ETM+)	6	440 to 2350	60 to 280	30	16
Landsat 8 (OLI)	8	435 to 2295	20 to 185	30	16
MODIS	7	459 to 2155	20 to 50	250 to 500	1 to 2
VIIRS	10	402 to 2275	15 to 60	750	1 to 2
AVHRR	3	580 to 1640	100 to 275	1090	1

[a] Spatial resolution is dependent on aircraft altitude and instrument IFOV.

atmospheric effects, sun-sensor geometry, and sensor radiometric resolution. However, this experiment is capable of illustrating the ability to characterize uncertainty in inversion results and improves the confidence with which we can extract information from lower quality data sources. Moreover, this experiment sets a theoretical limit on the accuracy and precision of leaf trait retrieval from spectral RTM inversion, thereby contextualizing past RTM inversion results (e.g. Zhang et al., 2005, 2006; 2009, & Zhang et al., 2012a,b) and guiding future research in the field.

The entire workflow for this paper is summarized in Fig. 1. The data and R source code for performing all analyses in this study have been made publicly available at github.com/ashiklom/sensor-manuscript. We encourage those interested to replicate our analyses and build on them with their own data and models.

3. Results

3.1. Validation

3.1.1. Reflectance and transmittance

For the inversion of synthetic spectra, we found no statistically significant ($p < 0.05$) spectral bias at any wavelength (Fig. S6). As well, the observed differences between input and simulated output were one to two orders of magnitude smaller than corresponding errors in the inversion of measured spectra (Fig. 2, Fig. S6). These results collectively illustrate that our algorithm is unbiased and contributes minimally to errors in the inversion of measured spectra.

For the inversion of measured spectra, we observed substantial variability in the spectral bias across all analyzed leaves, resulting in

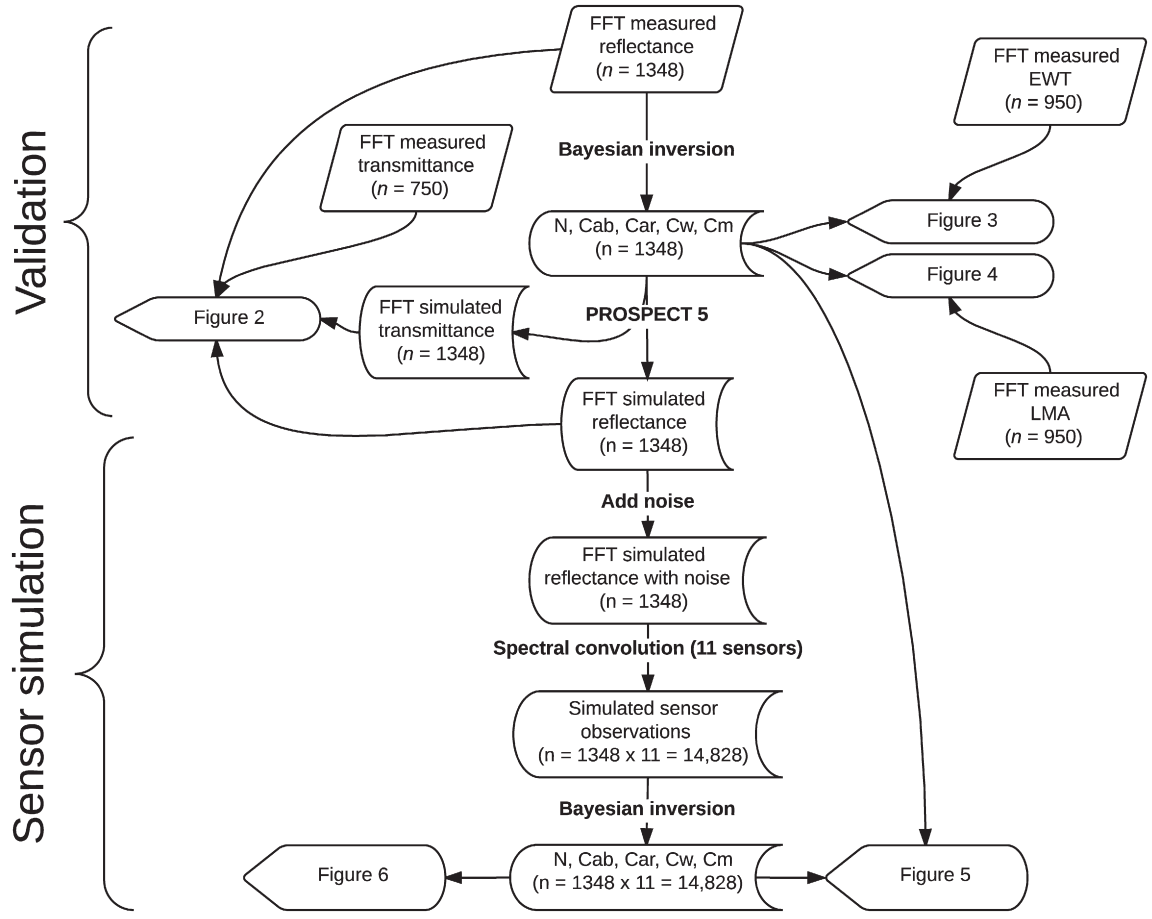

Fig. 1. Workflow illustrating the steps in this study as well as the figs. to which they correspond.

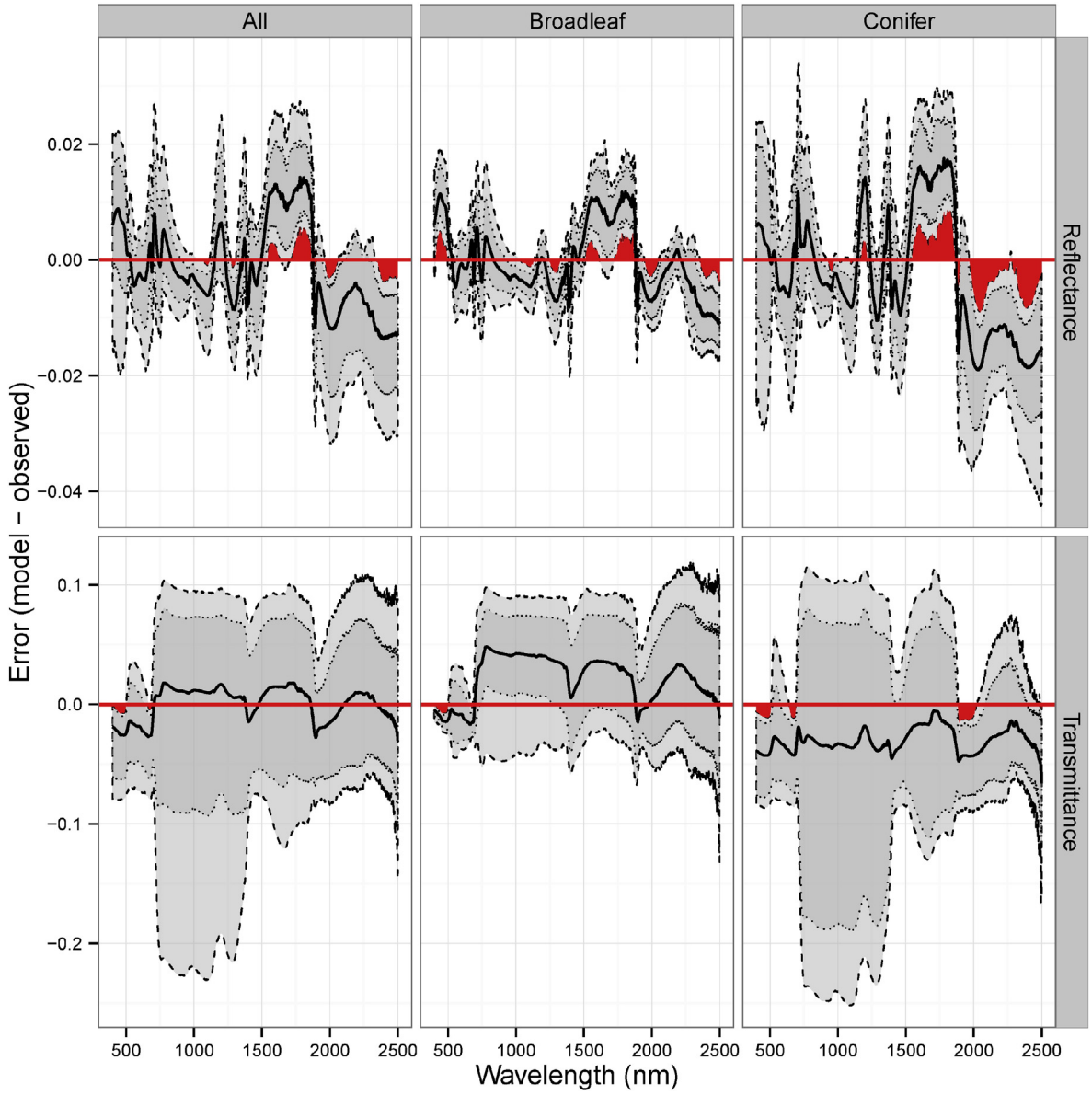

Fig. 2. Bias in FFT simulated reflectance (top) and transmittance (bottom) spectra compared to measurements over all leaves (left) and only hardwood (middle) and conifer (right) species. For a given wavelength, the solid black line is the mean bias, the dark grey bounded by the dotted line is the 90% confidence interval, the light grey region bounded by the dashed line is the 95% confidence interval, the red line highlights a bias of 0, and the red shaded regions highlight bias significant at the 95% confidence level.

Table 3
Reflectance (Refl.) and transmittance (Tran.) spectral validation error statistics aggregated across the visible (400–800 nm) and infrared (801–2500 nm) regions. Values from other studies are included for comparison.

		Visible			Infrared		
		RMSE	BIAS	SEPC	RMSE	BIAS	SEPC
Refl.	FFT all	0.0083	0.0018	0.0071	0.0098	−0.0020	0.0061
	Broadleaf	0.0063	0.0023	0.0042	0.0064	−0.0009	0.0034
	Conifer	0.0101	0.0011	0.0090	0.0127	−0.0035	0.0064
	Feret et al. (2008): CALMIT	0.032	0.010	0.028	–	–	–
	ANGERS	0.019	0.001	0.019	0.016	0.003	0.014
	HAWAII	0.021	−0.008	0.020	0.036	−0.031	0.017
	Di Vittorio (Di Vittorio, 2009a,b)	0.0255	0.00477	–	–	–	–
Tran.	FFT all	0.0404	−0.0133	0.0336	0.0551	0.0040	0.0537
	Broadleaf	0.0248	0.0012	0.0167	0.0450	0.0266	0.0336
	Conifer	0.0553	−0.0346	0.0389	0.0661	−0.0293	0.0566
	Feret et al. (2008): CALMIT	0.029	−0.005	0.025	–	–	–
	ANGERS	0.018	−0.005	0.017	0.016	0.001	0.015
	HAWAII	0.022	0.003	0.020	0.020	−0.003	0.017
	Di Vittorio (2009a,b)	0.0442	0.0294	–	–	–	–

statistically significant ($p < 0.05$) bias in only a few specific wavelength regions (Fig. 2). For both broadleaf and needle-leaf conifer species, reflectance was typically overestimated between 1600 and 1900 nm and underestimated between 1000 and 1300 nm and between 2000 and 2500 nm. The errors in the 1600 to 1900 nm and 2000 to 2500 nm ranges covered more wavelengths and had larger magnitude for conifer species than broadleaved species. Broadleaved species also had a statistically significant reflectance overestimate in the 400 to 500 nm range and an underestimate at 1300 nm, while conifer species had a significant reflectance overestimate at 1300 nm.

For both measured and synthetic spectra, transmittance bias (BIAS = −0.0133) was, on average, greater in magnitude than reflectance bias (BIAS = 0.0018), with a mean positive bias for broadleaved species (BIAS = 0.0012) and a mean negative bias for conifer species (BIAS = −0.0346) (Fig. 2, Table 3). However, the between-leaf variability in bias was also large and resulted in statistically significant bias in only a small number of specific spectral regions. For both broadleaved and conifer species, we observed a significant underestimate in transmittance in the chlorophyll *a* absorption 400 and 500 nm. Specifically for conifer species, we also observed underestimates in transmittance at the vegetation "red edge" around 700 nm and at a water absorption feature around 1900 nm.

3.1.2. EWT and LMA

Similar to the results of the spectral validation (Section 3.1.1), the inversion estimates of Cw and Cm (compared to measured values of EWT and LMA, respectively) displayed higher accuracy for broadleaf (CV_{Cw} = 18.8%, CV_{Cm} = 24.5%) versus conifer species (CV_{Cw} = 52.3%, CV_{Cm} = 63.3%) (Table 4). For the broadleaved species, our parameter estimates were within the range observed previously (Table 4). While the inversion estimates for conifer species show a lower performance compared to broadleaf trees, the error inversion results were primarily driven by a single plant functional type—early successional conifers, which consisted entirely of pine species (*Pinus* family). Notably, a few estimates for mid-successional conifer species displayed significant divergence with observations, but in general fell along the 1:1 relationship (Figs. 3 and 4).

3.2. Sensor simulation experiment

3.2.1. Parameter error

Across all of the selected sensors, the highest PROSPECT 5 parameter inversion uncertainty and bias were observed for Car (Fig. 5, Table 5). This can readily be explained by the Car specific absorption feature, which is both extremely narrow and overlaps substantially with that of Cab (Fig. S1). On the other extreme, the most accurate and least uncertain retrieved parameter was N, which is related to the reflectivity of the leaf across the entire spectrum (Fig. 5, Table 5, Fig. S1). Despite relatively narrow absorption features, most simulated sensors were able to retrieve Cab with reasonably good accuracy, which is not surprising given the long history of monitoring vegetation pigmentation using various platforms. Similarly, all sensors except CHRIS-Proba and AVHRR retrieved Cw with low uncertainty and bias, reflecting the wide and strong absorption features of water in the NIR and SWIR (Fig. 5, Table 5, Fig. S1). The failure of CHRIS-Proba to retrieve Cw can be attributed to its inability to measure in this spectral range (Fig. S4). The retrieval accuracy for Cm was much more sensor dependent, with good performance among the simulated hyperspectral sensors, VIIRS, and Landsat 8, followed by lower performance for simulated Landsat 5 and 7 and MODIS, and a poor result for the simulated Chris-PROBA and AVHRR data (Fig. 5, Table 5). Although the specific absorption feature for Cm is very wide, the sensitivity of reflectance to Cm values is much lower than for other parameters and almost the entire feature can be masked or confounded by Cw (Fig. S1). This suggests that Cm is very dependent on precise locations of certain bands and therefore explains the differences in the estimate accuracy of apparently similar sensors like Landsat 5, 7, and 8 (Table 2, Fig. S4). More generally, the importance of precise band widths and locations is evidenced by the noticeably better performance of Landsat 8 compared to Landsat 5 and 7 for certain parameters (Fig. 5, Table 5) despite the subtle differences in the sensors' respective bandwidths (Table 2, Fig. S4).

Table 4
Error statistics for the comparison of inversion estimates of PROSPECT parameters Cw and Cm and measured values of equivalent water thickness (EWT) and leaf dry mass per unit area (LMA), respectively. Values from other inversion studies are included for comparison.

		RMSE	BIAS	SEPC	CV	RMS%E
Cw/EWT ($g\ m^{-2}$)	FFT Broadleaf	17	5	16	18.8	21.64
	Conifer	187	90	164	52.3	67.29
	Feret et al. (2008): LOPEX	17	−3	17	15.2	–
	ANGERS	20	−1	20	17.1	–
	HAWAII	57	−15	55	19.8	–
	Féret et al. (2011): #3	27	–	–	–	–
	Li and Wang (2011)	12	5	–	20.10	–
Cm / LMA ($g\ m^{-2}$)	FFT Broadleaf	20	−18	9	24.5	43.75
	Conifer	121	35	116	61.6	65.51
	Feret et al. (2008): LOPEX	34	21	27	51.0	–
	ANGERS	26	1	26	49.8	–
	HAWAII	49	−35	35	27.8	–
	Féret et al. (2011): #3	31	–	–	–	–
	Li and Wang (2011)	8	−7	–	13.75	–

3.2.2. Parameter uncertainty and covariance

Fig. 6 shows an example of processed inversion output based on the high spectral resolution field spectrometer data and the spectral response functions of AVIRIS NG, Landsat 8, and MODIS. All four plots are simulated from a single set of parameters, so differences in results are caused only by variations in spectral measurement characteristics (Fig. S4). Out of these four sensors, the uncertainties increase with approximately decreasing spectral resolution, with lowest uncertainties in the full spectra, second-lowest for AVIRIS NG, second highest for Landsat 8, and highest for MODIS. The shapes of parameter covariances are distinctly different between these sensors, reflecting differences in the ability of the inversion to distinguish between parameters based on the available information. Across all four sensors, we observe strong positive covariance between N and Cm, since these parameters influence wide regions of the reflectance spectrum in opposite ways (Fig. S1). Similarly, we also observe a positive covariance between N and Cab, although the strength of this covariance is not equal across sensors. The remaining covariances are mostly specific to MODIS, whose band configuration increases the overlap between the associated parameters (Fig. S4).

We find that inversion estimates for the field spectra are occasionally falsely overconfident. For instance, the true value of N and Cw is outside the 95% confidence limit of their estimated joint probability distribution at full, field spectrometer resolution. That being said, this is less of an issue for the other sensors, where the joint probability distribution encompasses the true value. This suggests that spectral resolution below 5 nm may not provide additional information content, particularly for the broad absorption features within leaves, because of the strong autocorrelation between adjacent wavelengths. More importantly, although the joint posterior probability distributions from Landsat 8 and MODIS appear wide, the resulting parameter values are constrained by an order of magnitude or more compared to the priors.

4. Discussion

In this manuscript, we reiterate the power of the Bayesian RTM inversion framework for using spectral data to characterize vegetation and monitor ecosystem dynamics. The use of a physically-based model to describe the interaction of light with different vegetation structural and biochemical components improves the extent to which such an approach can be generalized across vegetation types and sub-

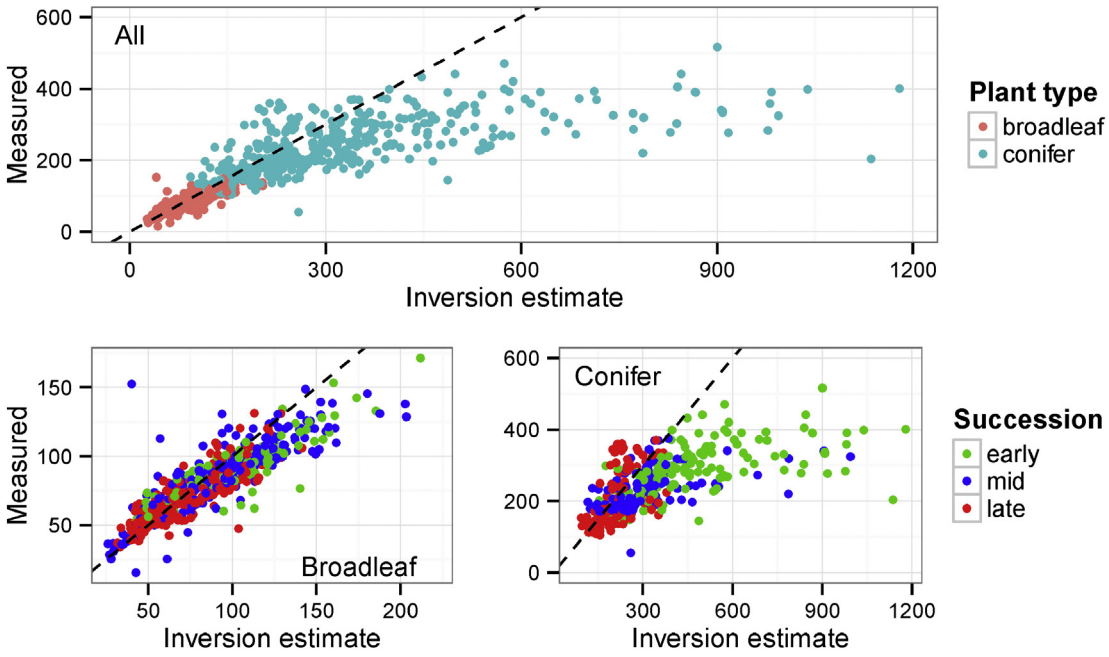

Fig. 3. Modeled and observed equivalent water thickness (g m^{-2}) for both conifers and hardwoods (a), just hardwoods (b), and just conifers (c). Point colors indicate plant type (a) or successional stage (b,c). The dashed line represents a 1:1 fit.

orbital and spaceborne platforms compared to more empirical approaches. Moreover, this physically-based approach enables estimation of vegetation properties from sensors of varying spectral resolution, and our ability to quantify uncertainty in our estimates provides the versatility to assess the performance of various sensors for a range of applications.

Our inversion results are comparable to other studies (Feret et al., 2008; Féret et al., 2011; Li & Wang, 2011; Di Vittorio, 2009a). The results outperformed those of Féret et al. (2011) despite the fact that we performed the inversion on measured spectra and inverted all five PROSPECT parameters, whereas Féret et al. (2011) performed inversions on synthetic spectra and did not attempt to estimate the structure parameter N. As such, we suggest that our approach does not come at the cost of model performance, and, importantly, enables the use of a much wider range of spectral data to explore vegetation dynamics. Our method contrasts with some previous methods (e.g. Feret et al., 2008; Féret et al., 2011) that utilize both reflectance and transmittance observations to invert leaf models such as PROSPECT. These require the use of additional, expensive instruments, such as an integrating sphere, that typically introduce significant noise and potential errors in the measurements given their inadequate design across a range of leaf habits. In addition, our approach suggests the possibility to instead use leaf reflectance observations alone to scale canopy-scale RTMs by coupling measured reflectance with simulated transmittance.

Placed in the context of past inversion studies, our work reveals some continuing challenges in the use of PROSPECT to model leaf optical

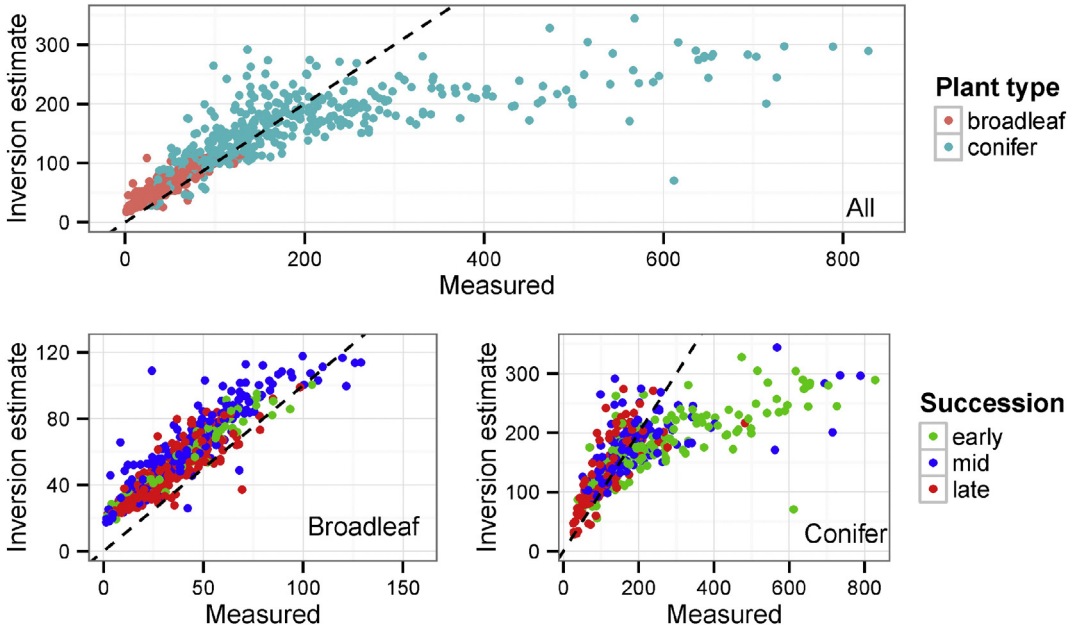

Fig. 4. Modeled and observed leaf dry mass per unit area (g m^{-2}) for both conifers and hardwoods (a), just hardwoods (b), and just conifers (c). Point colors indicate plant type (a) or successional stage (b,c). The dashed line represents a 1:1 fit.

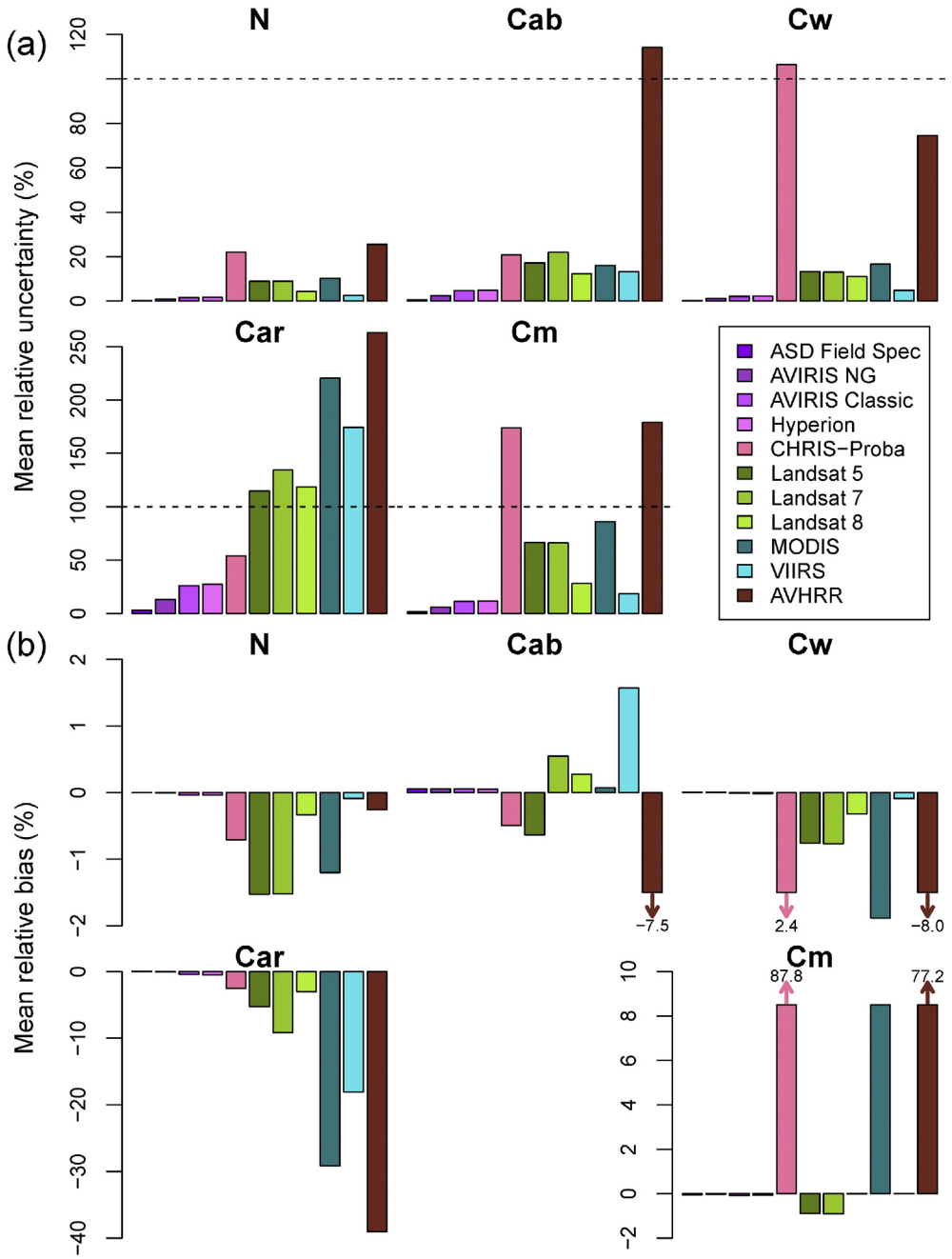

Fig. 5. Mean uncertainty (a) and relative bias (b) (as defined in Section 2.3) of inversion estimates for each parameter and simulated sensor. Sensors are arranged along the x-axis in approximate order of increasing spectral resolution.

Table 5
Uncertainty and relative bias in parameter estimates from inversion of simulated spectra filtered through relative spectral response curves of different sensors.

	Uncertainty (π)					Relative bias (α)				
Sensor	N	Cab	Car	Cw	Cm	N	Cab	Car	Cw	Cm
ASD Field Spec	0.20	0.54	2.91	0.26	1.33	−0.001	0.05	0.08	0.01	−0.05
AVIRIS NG	0.87	2.36	12.78	1.12	5.81	−0.004	0.05	−0.03	0.004	−0.03
AVIRIS Classic	1.62	4.61	26.06	2.13	11.02	−0.04	0.06	−0.44	−0.01	−0.08
Hyperion	1.69	4.81	27.35	2.23	11.44	−0.04	0.05	−0.49	−0.02	−0.06
CHRIS-Proba	21.93	20.77	53.86	106.5	173.8	−0.71	−0.50	−2.52	2.41	87.84
Landsat 5	8.90	17.14	114.8	13.32	66.43	−1.53	−0.64	−5.16	−0.76	−0.89
Landsat 7	8.84	21.90	134.2	12.94	66.07	−1.52	0.55	−9.17	−0.77	−0.91
Landsat 8	4.31	12.23	118.5	11.05	27.99	−0.33	0.28	−3.02	−0.32	−0.005
MODIS	10.29	15.99	220.5	16.65	86.00	−1.20	0.07	−29.14	−1.88	5.43
VIIRS	2.49	13.24	174.4	4.75	18.23	−0.09	1.57	−18.06	−0.09	0.004
AVHRR	25.47	114.2	263.3	74.58	179.1	−0.26	−7.47	−39.04	−8.04	77.21

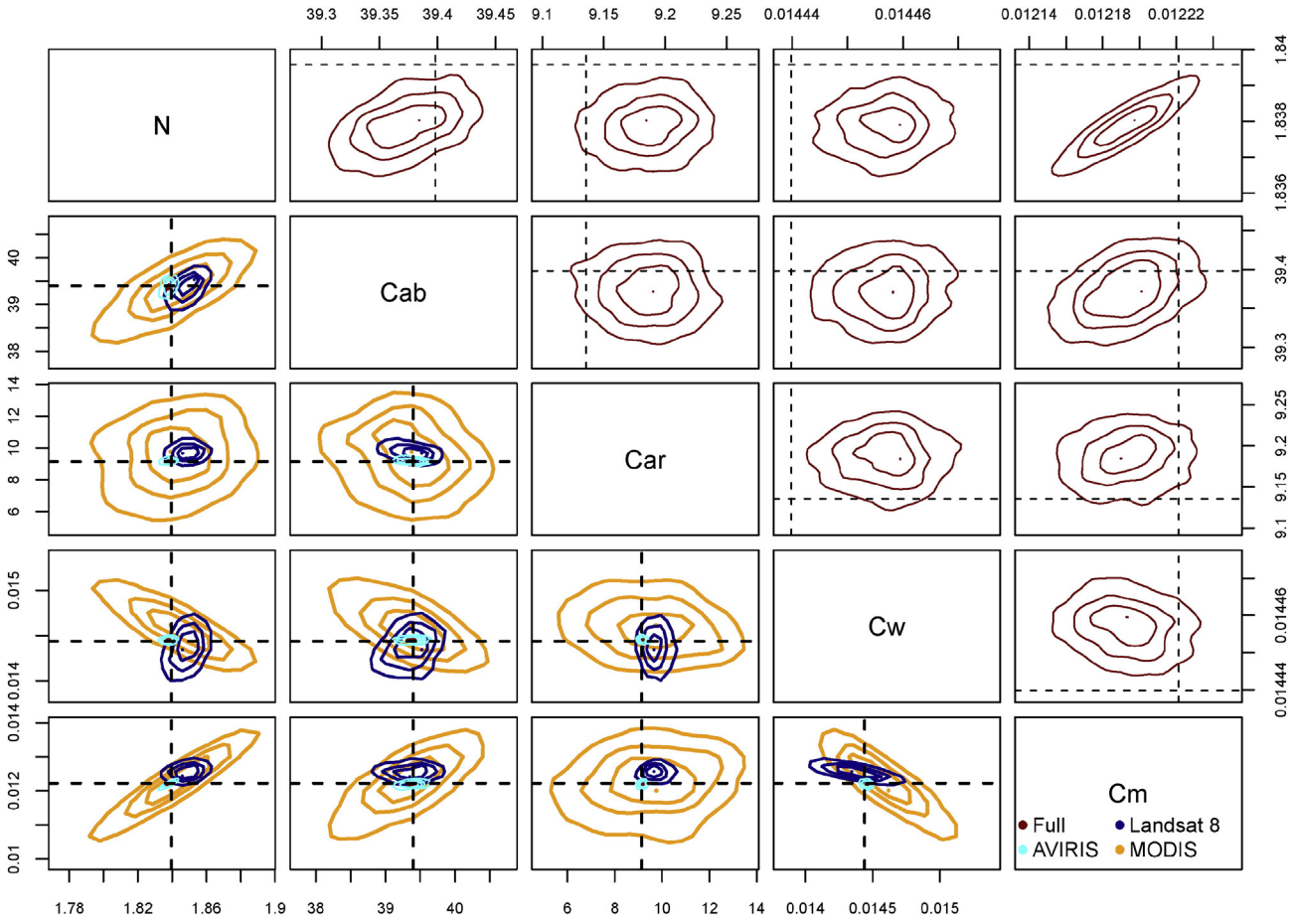

Fig. 6. Example joint probability distribution for parameter inversion estimates of simulated spectra using the full spectra (red; top panels) and the relative spectral response (RSR) functions of AVIRIS NG (cyan), Landsat 8 (dark blue), and MODIS (orange). Dotted lines indicate true parameter values. Note that the axis range of the top panels is substantially smaller than that of the bottom panels. (For interpretation of the references to color in this figure legend, the reader is referred to the web version of this article.)

properties and provides some guidance for future RTM development. For instance, we noted issues with using PROSPECT to model reflectance and transmittance in the 400 to 500 nm range (Fig. 2) that have also been reported in previous studies. Feret et al. (2008) observed a consistently negative transmittance bias and occasionally a positive or negative reflectance bias. Similarly, Croft, Chen, Zhang, and Simic (2013) report systematic underestimates of reflectance in this part of the spectrum. One possible source of bias is PROSPECT's simplified description of leaf structure (Jacquemoud & Baret, 1990) and failure to account for specular reflectance off the leaf surface (Grant, 1987). Another possible source of error is imprecise calibration of the leaf refractive index, which has a relatively strong wavelength dependence in the region of interest (400–500 nm) (Feret et al., 2008). Alternatively, this bias could be the result of the failure of the PROSPECT 5 model to properly represent the spectral properties of chlorophyll in leaves, potentially requiring additional calibration across a broader range of species and environments. The common specific absorption feature for chlorophyll *a* and *b* ($k_{Cab}(\lambda)$) in PROSPECT 5 used in this study is empirically calibrated to a single data set (ANGERS; Feret et al., 2008), and many studies have shown that this feature may need to be re-calibrated to the data at hand to obtain accurate inversion estimates, particularly for species dissimilar to those in the ANGERS data set (Malenovský et al., 2006; Moorthy, Miller, & Noland, 2008; Zhang, Chen, Miller, & Noland, 2008; Li & Wang, 2013). As well, PROSPECT 5 fails to distinguish between chlorophyll *a* and *b*, which have overlapping but distinctly different absorption signatures and whose ratios have been shown to be affected by environmental conditions (Blackburn, 2007; Di Vittorio, 2009b; Di Vittorio & Biging, 2009). Fortunately, it has been shown that not only can chlorophyll *a* and *b* be distinguished using imaging spectroscopy (Di Vittorio, 2009b), but that these differences can be incorporated into a RTM to improve its performance (Di Vittorio, 2009a).

Reflectance in the SWIR region (>1500 nm)—where we observed significant reflectance bias (Fig. 2)—is influenced by three PROSPECT parameters: N, Cw, and Cm (Fig. S1). All three parameters modulate reflectance in this spectral region monotonically: Reflectance increases with higher values of N and decreases with higher values of Cw and Cm (Fig. S1). This means that it is unlikely that incorrect parameter trade-off within the algorithm (e.g. preferentially selecting Cw over Cm) could contribute to this error. Feret et al. (2008) also reported similar reflectance bias patterns for the ANGERS data set despite using a different inversion methodology. We hypothesize this bias is the result of PROSPECT's insufficient characterization of the specific absorption spectrum of leaf dry matter ($k_{Cm}(\lambda)$), since the absorption characteristics of water ($k_{Cw}(\lambda)$) are very well known and N is not dependent on an absorption feature. This would also help explain the negative bias we observed between spectral inversion estimates of Cm and direct measurements of LMA (Fig. 3, Table 3). Other studies have also reported a bias but the direction of this bias has not been consistent, with some studies showing negative bias across all their data (Li & Wang, 2011; Cheng et al., 2014) and others reporting a bias whose magnitude and direction is data-dependent (Feret et al., 2008). This may partially be explained by the simple treatment of non-pigment compounds in the current PROSPECT model, wherein protein, cellulose, hemicellulose, sugar, starch, and lignin are aggregated into a single parameter (Cm) (Fourty, Baret, Jacquemoud, Schmuck, & Verdebout, 1996). As with chlorophyll, the absorption feature for Cm is empirically derived

(Feret et al., 2008) and fails to represent variability in the relative abundance of the different components (Poorter et al., 2009). Fortunately, Wang, Skidmore, Wang, Darvishzadeh, and Hearne (2015) demonstrated that, with proper calibration, it is possible to use PROSPECT inversion to determine leaf protein as well as combined cellulose and lignin content. Furthermore, measurements of LMA are an aggregate of a number of constituents including chlorophyll, carotenoids, lipids, organic acids, phenolics, and vascular tissue (Poorter et al., 2009), which would positively bias the measurement compared to the spectral estimate. Finally, it is possible that strong positive covariance between N and Cm (Fig. 6) caused by their significant spectral overlap (Fig. S1) interferes with accurate estimation of Cm. However, based on our finding that inversions of simulated spectra did not display this problem (Field spectra in Fig. 5; Fig. S6), we conclude the error is in fact driven more by model formulation than by parameter identifiability. We are aware of only one other study that attempted to estimate all five PROSPECT parameters (including the structure parameter, N) simultaneously: Li and Wang (2011) presented a novel algorithm for PROSPECT inversion that assigns a separate merit function to each parameter (rather than a single common merit function for all parameters) and demonstrated its improved performance over traditional approaches. However, although their new algorithm reduced error and bias in the LMA estimates, a negative bias comparable to the one we report still remained across all of their data sets.

Based on these results, we suggest that future PROSPECT development should aim for finer distinction in leaf chemical components. That being said, the introduction of additional parameters into a model must be approached with caution, as parameter precision and identifiability tend to decrease with model complexity. The ability of our Bayesian inversion to quantify parameter uncertainty and covariance makes it useful for nested model selection. An alternative approach to addressing the issue of empirically-calibrated absorption coefficients is to explicitly account for their uncertainty and covariance structures. Within our Bayesian framework, such uncertainties could be treated as observation errors and propagated to the uncertainty in parameter estimates. In subsequent work, we will explore such a calibration using coupled spectral-trait data from multiple available datasets.

The relatively large magnitude in our observed transmittance bias (compared to reflectance) is likely the result of using only reflectance as input in our inversion. A combined approach using measured reflectance and transmittance observations, collected on the same leaf samples, may have shown the variability distributed more evenly because the minimization of the residuals would have been more balanced between the two vectors of data. Ultimately, higher uncertainties in transmittance estimates compared to reflectance are a consequence of the inherent challenges in using integrating spheres to measure transmittance, especially the substantial noise in the SWIR regions. This is supported by the absence of significant systematic bias between measured and modeled transmittance across the overwhelming majority of the spectrum (Fig. 2). Moreover, although the confidence intervals on transmittance bias are as high as 25% at some wavelengths, averaging over all spectra and aggregating across the visible (400 to 800 nm) and infrared (801 to 2500 nm) regions leads to results similar to those reported in other field spectra inversion studies, even though these studies used both reflectance and transmittance as input (Table S1). Although our overall transmittance RMSE values were two to three times higher than those reported by Feret et al. (2008), these errors are inflated by the inclusion of conifer species, for which reflectance is harder to measure reliably and the assumptions of the PROSPECT model are not satisfied (Jacquemoud & Baret, 1990; Di Vittorio, 2009a; Allen, Gausman, Richardson, & Thomas, 1969). As well, measurements of needle-leaf transmittance often result in considerable noise in longer wavelengths (SWIR, >2000 nm) given the physical challenges of making these measurements on needle-leaf species (and other leaf types), generally poor lamp performance as compared to other methods, and the much smaller transmission of light in these wavelengths (often resulting in signals below the precision of the instrument). As such we would expect higher reported error compared to other leaf morphologies. For example, in examining our broadleaf samples we observed that the statistics for transmittance are much closer to those reported by Feret et al. (2008), despite not including measured transmittance in the inversion (Table S1). Our transmittance error statistics are also similar to those reported for conifers by Di Vittorio (2009a) who used transmittance information and a re-calibrated version of the LIBERTY leaf RTM (Table 3). Moreover, our reflectance statistics show error comparable to or lower than those reported in similar studies (Feret et al., 2008; Di Vittorio, 2009a).

Through our sensor experiment, we explicitly demonstrate the tradeoffs between spectral information content and parameter uncertainty and identifiability. With increasingly coarse spectral resolution, we observed not only wider parameter confidence intervals indicating higher uncertainty but also tighter covariance structures indicating a reduced ability to distinguish between parameters (Fig. 6). This comparison approach can be used to guide future enhancements of radiative transfer models by quantitatively showing whether a model of a given complexity is warranted given data of a particular quality. For example, in our simulation experiment, all the full-range hyperspectral sensors were capable of accurately estimating chlorophyll and carotenoids, but the ability of multispectral sensors to do so was dramatically lower (Figs. 5, S6, and S7; Table 5). We therefore can conclude that the use of PROSPECT 5 is warranted when performing inversion of hyperspectral data, but PROSPECT 4 (which does not distinguish between pigments) may be preferable for multispectral data. A similar framework can be used to determine the utility of increasingly complex future versions of PROSPECT that further differentiate leaf biochemical and structural components.

Importantly, the results of our sensor simulation experiment are highly idealized due to their failure to consider canopy structure, atmospheric effects, sun-sensor geometry, and sensor radiometric and spatial characteristics. However, a similar Bayesian inversion framework has been shown to work on MODIS data for the related coupled leaf-canopy RTM PROSAIL (Zhang et al., 2005, 2006; Zhang et al., 2009, & Zhang et al., 2012a; Zhang, Qu, Wang, Liang, & Liu, 2012b) and we believe the framework can be readily applied to other RTMs that address many of the limitations of our study. In future work, we will explore Bayesian spectral inversion of the coupled leaf-canopy RTM responsible for energy balance calculations in the ED2 ecosystem model (Medvigy et al., 2009) on atmospherically corrected and orthorectified AVIRIS imagery, which will be an important milestone in bringing together the remote sensing and ecological modeling communities. In the long run, our framework could also be extended to the inversion of coupled canopy-atmosphere models using a combination of meteorological and spectral data from Earth Observation satellites, leveraging the relative advantages of each platform to generate unified time series of ecologically meaningful parameters with unprecedented spatial and temporal resolution.

5. Conclusions

This study introduces a novel application of Bayesian spectral inversion to the PROSPECT 5 leaf RTM that explicitly takes into account uncertainty and correlation in parameter estimates. Validation of our algorithm on a coupled leaf spectral-trait database revealed accuracy comparable to previous inversion algorithms despite only using reflectance observations and the default PROSPECT model (i.e. no additional refinement of the specific absorption features). By simulating reflectance measurements with the spectral characteristics of different remote sensing platforms, we were able to quantify the relationship between spectral resolution and parameter uncertainty. Although our simulated observations are highly idealized, we believe the resulting patterns in retrieved parameter accuracy and precision are representative of the advantages and limitations of the spectral configurations of

different sensors for remote sensing of vegetation. Our work reinforces the notion that Bayesian spectral inversion provides a powerful and versatile framework for future RTM development and single- and multi-instrumental remote sensing of vegetation, and we encourage members of the remote sensing community to apply and build upon the tools we have developed (which can be viewed and downloaded at https://github.com/PecanProject/pecan/tree/master/modules/rtm).

Acknowledgements

This work is supported by NASA Grant NNX14AH65G and the Boston University Department of Earth & Environment. Field data collection was supported by NASA Grant NNX08AN31. We would also like to thank Sarah Weiskopf, Afshin Pourmokhtarian, Elizabeth Cowdery, Joshua Mantooth, and especially Christine Rollinson for their generous feedback on the content, style, and organization of this paper.

Appendix A. Supplementary data

Supplementary data to this article can be found online at http://dx.doi.org/10.1016/j.rse.2016.05.023.

References

Allen, W. A., Gausman, H. W., Richardson, A. J., & Thomas, J. R. (1969). Interaction of isotropic light with a compact plant leaf. *Journal of the Optical Society of America*, *59*(10), 11–14.

Asner, G. P., Martin, R. E., Anderson, C. B., & Knapp, D. E. (2015). Quantifying forest canopy traits: Imaging spectroscopy versus field survey. *Remote Sensing of Environment*, *158*, 15–27 (http://doi.org/10.1016/j.rse.2014.11.011).

Atzberger, C., & Richter, K. (2012). Spatially constrained inversion of radiative transfer models for improved LAI mapping from future sentinel-2 imagery. *Remote Sensing of Environment*, *120*, 208–218 (http://doi.org/10.1016/j.rse.2011.10.035).

Banskota, A., Wynne, R. H., Serbin, S. P., Kayastha, N., Thomas, V. A, & Townsend, P. A. (2013). Utility of the wavelet transform for LAI estimation using hyperspectral data. Photogrammetric Engineering and Remote Sensing, 79(7), 7907.

Banskota, A., Serbin, S. P., Wynne, R. H., Thomas, V. A., Falkowski, M. J., Kayastha, N., & Townsend, P. A. (2015). An LUT-based inversion of DART model to estimate forest LAI from hyperspectral data. *IEEE Journal of Selected Topics in Applied Earth Observations and Remote Sensing*, 1–14.

Blackburn, G. A. (2007). Hyperspectral remote sensing of plant pigments. *Journal of Experimental Botany*, *58*(4), 855–867. http://dx.doi.org/10.1093/jxb/erl123.

Blackburn, G. A., & Ferwerda, J. G. (2008). Retrieval of chlorophyll concentration from leaf reflectance spectra using wavelet analysis. *Remote Sensing of Environment*, *112*(4), 1614–1632. http://dx.doi.org/10.1016/j.rse.2007.08.005.

Cheng, T., Rivard, B., Sánchez-Azofeifa, G. A., Feng, J., & Calvo-Polanco, M. (2010). Continuous wavelet analysis for the detection of green attack damage due to mountain pine beetle infestation. *Remote Sensing of Environment*, *114*(4), 899–910. http://dx.doi.org/10.1016/j.rse.2009.12.005.

Cheng, T., Rivard, B., Sánchez-Azofeifa, A. G., Féret, J. B., Jacquemoud, S., & Ustin, S. L. (2014). Deriving leaf mass per area (LMA) from foliar reflectance across a variety of plant species using continuous wavelet analysis. *ISPRS Journal of Photogrammetry and Remote Sensing*, *87*, 28–38. http://dx.doi.org/10.1016/j.isprsjprs.2013.10.009.

Combal, B., Baret, F., Weiss, M., Trubuil, A., Macé, D., Pragnère, A., ... Wang, L. (2003). Retrieval of canopy biophysical variables from bidirectional reflectance using prior information to solve the ill-posed inverse problem. *Remote Sensing of Environment*, *84*(1), 1–15. http://dx.doi.org/10.1016/S0034-4257(02)00035-4.

Couture, J. J., Serbin, S. P., & Townsend, P. A. (2013). Spectroscopic sensitivity of real-time, rapidly induced phytochemical change in response to damage. *New Phytologist*, *198*(1), 311–319. http://dx.doi.org/10.1111/nph.12159.

Cressie, N., Calder, C. A., Clark, J. S., Ver Hoef, J. M., & Wikle, C. K. (2009). Accounting for uncertainty in ecological analysis: The strengths and limitations of hierarchical statistical modeling. *Ecological Applications*, *19*(3), 553–570. http://dx.doi.org/10.1890/07-0744.1.

Croft, H., Chen, J. M., Zhang, Y., & Simic, A. (2013). Modelling leaf chlorophyll content in broadleaf and needle leaf canopies from ground, CASI, Landsat TM 5 and MERIS reflectance data. *Remote Sensing of Environment*, *133*, 128–140. http://dx.doi.org/10.1016/j.rse.2013.02.006.

Croft, H., Chen, J. M., & Zhang, Y. (2014). The applicability of empirical vegetation indices for determining leaf chlorophyll content over different leaf and canopy structures. *Ecological Complexity*, *17*(1), 119–130. http://dx.doi.org/10.1016/j.ecocom.2013.11.005.

Dawson, T. P., Curran, P. J., & Plummer, S. E. (1998). LIBERTY - Modeling the effects of leaf biochemical concentration on reflectance spectra. *Remote Sensing of Environment*, *65*(1), 50–60. http://dx.doi.org/10.1016/S0034-4257(98)00007-8.

Deel, L. N., McNeil, B. E., Curtis, P. G., Serbin, S. P., Singh, A., Eshleman, K. N., & Townsend, P. a. (2012). Relationship of a Landsat cumulative disturbance index to canopy nitrogen and forest structure. *Remote Sensing of Environment*, *118*, 40–49. http://dx.doi.org/10.1016/j.rse.2011.10.026.

Di Vittorio, A. V. (2009a). Enhancing a leaf radiative transfer model to estimate concentrations and in vivo specific absorption coefficients of total carotenoids and chlorophylls a and b from single-needle reflectance and transmittance. *Remote Sensing of Environment*, *113*(9), 1948–1966. http://dx.doi.org/10.1016/j.rse.2009.05.002.

Di Vittorio, A. V. (2009b). Pigment-based identification of ozone-damaged pine needles as a basis for spectral segregation of needle conditions. *Journal of Environmental Quality*, *38*(3), 855–867. http://dx.doi.org/10.2134/jeq2008.0260.

Di Vittorio, A. V., & Biging, G. S. (2009). Spectral identification of ozone-damaged pine needles. *International Journal of Remote Sensing*, *30*(12), 3041–3073. http://dx.doi.org/10.1080/01431160802558725.

Dietze, M. C., & Moorcroft, P. R. (2011). Tree mortality in the eastern and Central United States: Patterns and drivers. *Global Change Biology*, *17*(11), 3312–3326. http://dx.doi.org/10.1111/j.1365-2486.2011.02477.x.

Dietze, M. C., Lebauer, D. S., & Kooper, R. (2013). On improving the communication between models and data. *Plant, Cell and Environment*, *36*(9), 1575–1585. http://dx.doi.org/10.1111/pce.12043.

Fassnacht, F. E., Stenzel, S., & Gitelson, A. A. (2015). Non-destructive estimation of foliar carotenoid content of tree species using merged vegetation indices. *Journal of Plant Physiology*, *176*, 210–217. http://dx.doi.org/10.1016/j.jplph.2014.11.003.

Feret, J. B., François, C., Asner, G. P., Gitelson, A. A., Martin, R. E., Bidel, L. P. R., ... Jacquemoud, S. (2008). PROSPECT-4 and 5: Advances in the leaf optical properties model separating photosynthetic pigments. *Remote Sensing of Environment*, *112*(6), 3030–3043. http://dx.doi.org/10.1016/j.rse.2008.02.012.

Féret, J. -B., François, C., Gitelson, A., Asner, G. P., Barry, K. M., Panigada, C., ... Jacquemoud, S. (2011). Optimizing spectral indices and chemometric analysis of leaf chemical properties using radiative transfer modeling. *Remote Sensing of Environment*, *115*(10), 2742–2750. http://dx.doi.org/10.1016/j.rse.2011.06.016.

Ferreira, M. P., Grondona, A. E. B., Rolim, S. B. A., & Shimabukuro, Y. E. (2013). Analyzing the spectral variability of tropical tree species using hyperspectral feature selection and leaf optical modeling. *Journal of Applied Remote Sensing*, *7*(1), 073502. http://dx.doi.org/10.1117/1.JRS.7.073502.

Fourty, T., Baret, F., Jacquemoud, S., Schmuck, G., & Verdebout, J. (1996). Leaf optical properties with explicit description of its biochemical composition: Direct and inverse problems. *Remote Sensing of Environment*, *56*(2), 104–117. http://dx.doi.org/10.1016/0034-4257(95)00234-0.

Friedl, M. A., McIver, D. K., Hodges, J. C. F., Zhang, X., Muchoney, D., Strahler, A. H., ... Schaaf, C. (2002). Global land cover mapping from MODIS: Algorithms and early results. *Remote Sensing of Environment*, *83*, 287–302. http://dx.doi.org/10.1016/S0034-4257(02)00078-0.

Ganapol, B. D., Johnson, L. F., Hammer, P. D., Hlavka, C. A., & Peterson, D. L. (1998). LEAFMOD: A new within-leaf radiative transfer model. *Remote Sensing of Environment*, *63*(2), 182–193. http://dx.doi.org/10.1016/S0034-4257(97)00134-X.

Gelman, A., & Rubin, D. B. (1992). Inference from iterative simulation using multiple sequences. *Statistical Science*, *7*, 457–511.

Grant, L. (1987). Diffuse and specular characteristics of leaf reflectance. *Remote Sensing of Environment*, *22*, 309–322. http://dx.doi.org/10.1016/0034-4257(87)90064-2.

Haario, H., Saksman, E., & Tamminen, J. (2001). An adaptive metropolis algorithm. *Bernoulli*, *7*(2), 223–242. http://dx.doi.org/10.2307/3318737.

Haboudane, D., Miller, J. R., Tremblay, N., Zarco-Tejada, P. J., & Dextraze, L. (2002). Integrated narrow-band vegetation indices for prediction of crop chlorophyll content for application to precision agriculture. *Remote Sensing of Environment*, *81*(2–3), 416–426. http://dx.doi.org/10.1016/S0034-4257(02)00018-4.

Hansen, M. C., Stehman, S. V., & Potapov, P. V. (2010). Quantification of global gross forest cover loss. *Proceedings of the National Academy of Sciences of the United States of America*, *107*(19), 8650–8655. http://dx.doi.org/10.1073/pnas.0912668107.

Houborg, R., Fisher, J. B., & Skidmore, A. K. (2015). Advances in remote sensing of vegetation function and traits. . *International Journal of Applied Earth Observation and Geoinformation*. http://dx.doi.org/10.1016/j.jag.2015.06.001.

Huete, A., Didan, K., Miura, T., Rodriguez, E. P., Gao, X., & Ferreira, L. G. (2002). Overview of the radiometric and biophysical performance of the MODIS vegetation indices. *Remote Sensing of Environment*, *83*(1–2), 195–213. http://dx.doi.org/10.1016/S0034-4257(02)00096-2.

Hunt, E. R. J., Wang, L., Qu, J. J., & Hao, X. (2012). Remote sensing of fuel moisture content from canopy water indices and normalized dry matter index. *Journal of Applied Remote Sensing*, 6. http://dx.doi.org/10.1117/1.JRS.6.061705.

Jacquemoud, S., & Baret, F. (1990). PROSPECT: A model of leaf optical properties spectra. *Remote Sensing of Environment*, *34*(2), 75–91. http://dx.doi.org/10.1016/0034-4257(90)90100-Z.

Jacquemoud, S., Baret, F., Andrieu, B., Danson, F. M., & Jaggard, K. (1995). Extraction of vegetation biophysical parameters by inversion of the PROSPECT + SAIL models on sugar beet canopy reflectance data. Application to TM and AVIRIS sensors. *Remote Sensing of Environment*, *52*(3), 163–172. http://dx.doi.org/10.1016/0034-4257(95)00018-V.

Jacquemoud, S., Verhoef, W., Baret, F., Bacour, C., Zarco-Tejada, P. J., Asner, G. P., ... Ustin, S. L. (2009). PROSPECT + SAIL models: A review of use for vegetation characterization. *Remote Sensing of Environment*, *113*(Suppl. 1), S56–S66. http://dx.doi.org/10.1016/j.rse.2008.01.026.

Knyazikhin, Y., Martonchik, J. V., Diner, D. J., Myneni, R. B., Verstraete, M., Pinty, B., & Gobron, N. (1998). Estimation of vegetation canopy leaf area index and fraction from atmosphere-corrected MISR data. *Journal of Geophysical Research*, *103*, 239–256.

Knyazikhin, Y., Schull, M. A., Stenberg, P., Mõttus, M., Rautiainen, M., Yang, Y., Marshak, A., Carmona, P. L., Kaufmann, R. K., Lewis, P., et al. (2013). Hyperspectral remote sensing of foliar nitrogen content. *Proceedings of the National Academy of Sciences of the United States of America*, *110*(3), E185–E192. http://dx.doi.org/10.1073/pnas.1210196109.

Kobayashi, H., Baldocchi, D. D., Ryu, Y., Chen, Q., Ma, S., Osuna, J. L., & Ustin, S. L. (2012). Modeling energy and carbon fluxes in a heterogeneous oak woodland: A three-dimensional approach. *Agricultural and Forest Meteorology*, *152*, 83–100.

Kuusk, A. (2001). A two-layer canopy reflectance model. *Journal of Quantitative Spectroscopy and Radiative Transfer*, *71*(1), 1–9. http://dx.doi.org/10.1016/S0022-4073(01)00007-3.

Laurent, V. C. E., Schaepman, M. E., Verhoef, W., Weyermann, J., & Chávez, R. O. (2014). Bayesian object-based estimation of LAI and chlorophyll from a simulated sentinel-2 top-of-atmosphere radiance image. *Remote Sensing of Environment*, *140*, 318–329. http://dx.doi.org/10.1016/j.rse.2013.09.005.

Lauvernet, C., Baret, F., Hascoët, L., Buis, S., & Le Dimet, F. X. (2008). Multitemporal-patch ensemble inversion of coupled surface-atmosphere radiative transfer models for land surface characterization. *Remote Sensing of Environment*, *112*(3), 851–861. http://dx.doi.org/10.1016/j.rse.2007.06.027.

Le Maire, G., François, C., & Dufrêne, E. (2004). Towards universal broad leaf chlorophyll indices using PROSPECT simulated database and hyperspectral reflectance measurements. *Remote Sensing of Environment*, *89*(1), 1–28. http://dx.doi.org/10.1016/j.rse.2003.09.004.

LeBauer, D. S., Wang, D., Richter, K. T., Davidson, C. S., & Dietze, M. C. (2013). Facilitating feedbacks between field measurements and ecosystem models. *Ecological Monographs*, *83*(2), 133–154.

Lepine, L. C., Ollinger, S. V., Ouimette, A. P., & Martin, M. E. (2016). Examining spectral reflectance features related to foliar nitrogen in forests: Implications for broad-scale nitrogen mapping. *Remote Sensing of Environment*, *173*, 174–186. http://dx.doi.org/10.1016/j.rse.2015.11.028.

Leprieur, C., Verstraete, M. M., & Pinty, B. (1994). Evaluation of the performance of various vegetation indices to retrieve vegetation cover from AVHRR data. *Remote Sensing Reviews*, *10*(4), 265–284. http://dx.doi.org/10.1080/02757259409532250.

Li, P., & Wang, Q. (2011). Retrieval of leaf biochemical parameters using PROSPECT inversion: A new approach for alleviating ill-posed problems. *IEEE Transactions on Geoscience and Remote Sensing*, *49*(7), 2499–2506. http://dx.doi.org/10.1109/TGRS.2011.2109390.

Li, P. H., & Wang, Q. (2013). Retrieval of chlorophyll for assimilating branches of a typical desert plant through inversed radiative transfer models. *International Journal of Remote Sensing*, *34*(7), 2402–2416. http://dx.doi.org/10.1080/01431161.2012.744859.

Liu, J., Pattey, E., & Jégo, G. (2012). Assessment of vegetation indices for regional crop green LAI estimation from Landsat images over multiple growing seasons. *Remote Sensing of Environment*, *123*, 347–358. http://dx.doi.org/10.1016/j.rse.2012.04.002.

Loveland, T. R., Reed, B. C., Brown, J. F., Ohlen, D. O., Zhu, Z., Yang, L., & Merchant, J. W. (2000). Development of a global land cover characteristics database and IGBP DISCover from 1 km AVHRR data. *International Journal of Remote Sensing*, *21*(6–7), 1303–1330. http://dx.doi.org/10.1080/014311600210191.

Malenovský, Z., Albrechtová, J., Lhoták ová, Z., Zurita-Milla, R., Clevers, J. G. P. W., Schaepman, M. E., & Cudlín, P. (2006). Applicability of the PROSPECT model for Norway spruce needles. *International Journal of Remote Sensing*, *27*(24), 5315–5340. http://dx.doi.org/10.1080/01431160600762990.

Medvigy, D., Wofsy, S. C., Munger, J. W., Hollinger, D. Y., & Moorcroft, P. R. (2009). Mechanistic scaling of ecosystem function and dynamics in space and time: Ecosystem demography model version 2. *Journal of Geophysical Research: Biogeosciences*, *114*(1), 1–21. http://dx.doi.org/10.1029/2008JG000812.

Moorthy, I., Miller, J. R., & Noland, T. L. (2008). Estimating chlorophyll concentration in conifer needles with hyperspectral data: An assessment at the needle and canopy level. *Remote Sensing of Environment*, *112*(6), 2824–2838. http://dx.doi.org/10.1016/j.rse.2008.01.013.

Mousivand, A., Menenti, M., Gorte, B., & Verhoef, W. (2015). Multi-temporal, multi-sensor retrieval of terrestrial vegetation properties from spectral-directional radiometric data. *Remote Sensing of Environment*, *158*, 311–330. http://dx.doi.org/10.1016/j.rse.2014.10.030.

Myneni, R. B., Hoffman, S., Knyazikhin, Y., Privette, J. L., Glassy, J., Tian, Y., Wang, Y., Song, X., Zhang, Y., Smith, G. R., et al. (2002). Global products of vegetation leaf area and fraction absorbed PAR from year one of MODIS data. *Remote Sensing of Environment*, *83*(1–2), 214–231. http://dx.doi.org/10.1016/S0034-4257(02)00074-3.

Ni-Meister, W., Yang, W., & Kiang, N. Y. (2010). A clumped-foliage canopy radiative transfer model for a global dynamic terrestrial ecosystem model. I: Theory. *Agricultural and Forest Meteorology*, *150*(7–8), 881–894. http://dx.doi.org/10.1016/j.agrformet.2010.02.009.

Pinty, B., Andredakis, I., Clerici, M., Kaminski, T., Taberner, M., Verstraete, M. M., ... Widlowski, J. -L. (2011). Exploiting the MODIS albedos with the two-stream inversion package (JRC-TIP): 1. Effective leaf area index, vegetation, and soil properties. *Journal of Geophysical Research: Atmospheres*, *116*, 1–20. http://dx.doi.org/10.1029/2010JD015372.

Plummer, M., Best, N., Cowles, K., Vines, K., Sarkar, D., & Almond, R. (2016). Coda: Output analysis and diagnostics for MCMC. https://cran.r-project.org/web/packages/coda/

Poorter, H., Niinemets, U., Poorter, L., Wright, I. J., & Villar, R. (2009). Causes and consequences of variation in leaf mass per area (LMA): A meta-analysis. *New Phytologist*, *182*, 565–588.

Quaife, T., Lewis, P., De Kauwe, M., Williams, M., Law, B. E., Disney, M., & Bowyer, P. (2008). Assimilating canopy reflectance data into an ecosystem model with an ensemble Kalman filter. *Remote Sensing of Environment*, *112*(4), 1347–1364. http://dx.doi.org/10.1016/j.rse.2007.05.020.

R Development Core Team (2008). *R: A language and environment for statistical computing*. Vienna: Austria.

Serbin, S. P. (2012). *Spectroscopic determination of leaf nutritional, morphological, and metabolic traits. PhD dissertation*. Madison, WI, USA: UW-Madison.

Serbin, S. P., Dillaway, D. N., Kruger, E. L., & Townsend, P. A. (2012). Leaf optical properties reflect variation in photosynthetic metabolism and its sensitivity to temperature. *Journal of Experimental Botany*, *63*(1), 489–502. http://dx.doi.org/10.1093/jxb/err294.

Serbin, S. P., Singh, A., McNeil, B. E., Kingdon, C. C., & Townsend, P. A. (2014). Spectroscopic determination of leaf morphological and biochemical traits for northern temperate and boreal tree species. *Ecological Applications*, *24*(September), 140401105029006. http://dx.doi.org/10.1890/13-2110.1.

Singh, A., Serbin, S. P., McNeil, B. E., Kingdon, C. C., & Townsend, P. A. (2015). *Imaging spectroscopy algorithms for mapping canopy foliar chemical and morphological traits and their uncertainties*. Ecological Applications.

Sullivan, F. B., Ollinger, S. V., Martin, M. E., Ducey, M. J., Lepine, L. C., & Wicklein, H. F. (2013). Foliar nitrogen in relation to plant traits and reflectance properties of New Hampshire forests. *Canadian Journal of Forest Research*, *43*(1), 18–27. http://dx.doi.org/10.1139/cjfr-2012-0324.

Verhoef, W. (1984). Light scattering by leaf layers with application to canopy reflectance modeling: The SAIL model. *Remote Sensing of Environment*, *16*(2), 125–141. http://dx.doi.org/10.1016/0034-4257(84)90057-9.

Wang, Q., & Li, P. (2013). Canopy vertical heterogeneity plays a critical role in reflectance simulation. *Agricultural and Forest Meteorology*, *169*, 111–121. http://dx.doi.org/10.1016/j.agrformet.2012.10.004.

Wang, Z., Skidmore, A. K., Wang, T., Darvishzadeh, R., & Hearne, J. (2015). Applicability of the PROSPECT model for estimating protein and cellulose + lignin in fresh leaves. *Remote Sensing of Environment*, *168*, 205–218. http://dx.doi.org/10.1016/j.rse.2015.07.007.

Wessels, K. J., van den Bergh, F., & Scholes, R. J. (2012). Limits to detectability of land degradation by trend analysis of vegetation index data. *Remote Sensing of Environment*, *125*, 10–22. http://dx.doi.org/10.1016/j.rse.2012.06.022.

Wright, I. J., Reich, P. B., Westoby, M., Ackerly, D. D., Baruch, Z., Bongers, F., Cavender-Bares, J., Chapin, T., Cornelissen, J. H. C., Diemer, M., et al. (2004). The worldwide leaf economics spectrum. *Nature*, *428*(6985), 821–827. http://dx.doi.org/10.1038/nature02403.

Yao, Y., Liu, Q., Liu, Q., & Li, X. (2008). LAI retrieval and uncertainty evaluations for typical row-planted crops at different growth stages. *Remote Sensing of Environment*, *112*(1), 94–106. http://dx.doi.org/10.1016/j.rse.2006.09.037.

Zarco-Tejada, P. J., Miller, J. R., Harron, J., Hu, B., Noland, T. L., Goel, N., ... Sampson, P. (2004). Needle chlorophyll content estimation through model inversion using hyperspectral data from boreal conifer forest canopies. *Remote Sensing of Environment*, *89*(2), 189–199. http://dx.doi.org/10.1016/j.rse.2002.06.002.

Zarco-Tejada, P. J., Guillén-Climent, M. L., Hernández-Clemente, R., Catalina, A., González, M. R., & Martín, P. (2013). Estimating leaf carotenoid content in vineyards using high resolution hyperspectral imagery acquired from an unmanned aerial vehicle (UAV). *Agricultural and Forest Meteorology*, *171-172*, 281–294. http://dx.doi.org/10.1016/j.agrformet.2012.12.013.

Zhang, Q., Xiao, X., Braswell, B., Linder, E., Baret, F., & Moore, B. (2005). Estimating light absorption by chlorophyll, leaf and canopy in a deciduous broadleaf forest using MODIS data and a radiative transfer model. *Remote Sensing of Environment*, *99*(3), 357–371. http://dx.doi.org/10.1016/j.rse.2005.09.009.

Zhang, Q., Xiao, X., Braswell, B., Linder, E., Ollinger, S., Smith, M. -L., ... Minocha, R. (2006). Characterization of seasonal variation of forest canopy in a temperate deciduous broadleaf forest, using daily MODIS data. *Remote Sensing of Environment*, *105*(3), 189–203. http://dx.doi.org/10.1016/j.rse.2006.06.013.

Zhang, Y., Chen, J. M., Miller, J. R., & Noland, T. L. (2008). Retrieving chlorophyll content in conifer needles from hyperspectral measurements. *Canadian Journal of Remote Sensing*, *34*(3), 296–310.

Zhang, Q., Middleton, E. M., Margolis, H. A., Drolet, G. G., Barr, A. A., & Black, T. A. (2009). Can a satellite-derived estimate of the fraction of PAR absorbed by chlorophyll (FAPARchl) improve predictions of light-use efficiency and ecosystem photosynthesis for a boreal aspen forest? *Remote Sensing of Environment*, *113*(4), 880–888. http://dx.doi.org/10.1016/j.rse.2009.01.002.

Zhang, Q., Middleton, E. M., Gao, B. C., & Cheng, Y. B. (2012a). Using EO-1 Hyperion to simulate HyspIRI products for a coniferous forest: The fraction of par absorbed by chlorophyll (fAPAR chl) and leaf water content (LWC). *IEEE Transactions on Geoscience and Remote Sensing*, *50*(5 PART 2), 1844–1852. http://dx.doi.org/10.1109/TGRS.2011.2169267.

Zhang, Y., Qu, Y., Wang, J., Liang, S., & Liu, Y. (2012b). Estimating leaf area index from MODIS and surface meteorological data using a dynamic Bayesian network. *Remote Sensing of Environment*, *127*, 30–43. http://dx.doi.org/10.1016/j.rse.2012.08.015.

Zhao, F., Guo, Y., Huang, Y., Reddy, K. N., Lee, M. A., Fletcher, R. S., & Thomson, S. J. (2014). Early detection of crop injury from herbicide glyphosate by leaf biochemical parameter inversion. *International Journal of Applied Earth Observation and Geoinformation*, *31*(1), 78–85. http://dx.doi.org/10.1016/j.jag.2014.03.010.